Arabian Journal of Chemistry (2023) **16**, 105271

King Saud University

Arabian Journal of Chemistry

www.ksu.edu.sa
www.sciencedirect.com

ORIGINAL ARTICLE

Photovoltaic response promoted via intramolecular charge transfer in pyrazoline-based small molecular acceptors: Efficient organic solar cells

Muhammad Khalid [a,b,*], Ayesha Mustafa [a,b], Sarfraz Ahmed [c], Muhammad Adnan Asghar [d], Tansir Ahamad [e], Ataualpa A.C. Braga [f], Suvash Chandra Ojha [g,*]

[a] *Institute of Chemistry, Khwaja Fareed University of Engineering & Information Technology, Rahim Yar Khan 64200, Pakistan*
[b] *Centre for Theoretical and Computational Research, Khwaja Fareed University of Engineering & Information Technology, Rahim Yar Khan 64200, Pakistan*
[c] *Wellman Center for Photomedicine, Harvard Medical School, Massachusetts General Hospital, Boston, MA 02114, United States*
[d] *Department of Chemistry, Division of Science and Technology, University of Education Lahore, Pakistan*
[e] *Department of Chemistry, College of Science, King Saud University, Saudi Arabia*
[f] *Departamento de Qu´ımica Fundamental, Instituto de Qu´ımica, Universidade de Saǫ Paulo, Av. Prof. Lineu Prestes, 748, Sao Paulo 05508-000, Brazil*
[g] *Department of Infectious Diseases, The Affiliated Hospital of Southwest Medical University, Luzhou 646000, China*

Received 21 March 2023; accepted 14 September 2023
Available online 19 September 2023

KEYWORDS

Pyrazoline-based molecules;
DFT;
Optical properties;
TDM;
Open circuit voltage

Abstract Herein, a series of pyrazoline based non-fullerene compounds (**THP1-THP8**) having ladder-like backbone was designed by structural modulation with various electron accepting moieties. The density functional theory (DFT) and time-dependent functional theory (TD-DFT) study was executed at M06/6-311G(d,p) level for structural optimization and to determine the electronic and optical characteristics of the pyrazoline based chromophores. The optimized structures were employed to execute frontier molecular orbital (FMO), transition density matrix (TDM), density of state (DOS), open circuit voltage (V_{oc}) and reorganization energy analyses at the aforementioned level of DFT to comprehend the photovoltaic (PV) response of **THP1-THP8**. The red-shifted absorption spectrum (512.861–584.555 *nm*) with reduced band gap (2.507–2.881 *eV*) allow considerable charge transferal from HOMO to LUMO in all the studied compounds. Global reactivity parameters (GRPs) demonstrated high softness with considerable reactivity in **THP1-THP8**. More-

* Corresponding authors.
E-mail addresses: khalid@iq.usp.br (M. Khalid), tahamed@ksu.edu.sa (T. Ahamad), suvash_ojha@swmu.edu.cn (S.C. Ojha).
Peer review under responsibility of King Saud University.

Production and hosting by Elsevier

https://doi.org/10.1016/j.arabjc.2023.105271

over, remarkable V_{oc} values (2.083–2.973 V) were noted for all the derivatives (**THP1-THP8**). However, **THP2** with lowest energy gap (2.364 eV), highest λ_{max} (617.482 nm) and softness (0.423 eV) values is considered good candidate among afore-said chromophores. Hence, the studied chromophores with efficient properties are appropriate for experimentalists in terms of manufacturing of efficient OSCs.

1. Introduction

Development in science and technology offers advanced methods to produce clean energy at an adaptable level (Wu et al., 2005). The scientific community of the contemporary world is directing its approach of energy generation from greenhouse gas emission technologies to eco-friendly power generation projects and photovoltaic energy is a pertinent alternate for this aim (Shafiq et al., 2023b; ul Ain et al., 2021). The most auspicious approach of transforming solar energy into electrical power is by using photovoltaic cells employing photoelectric effect (Khalid et al., 2022a). Photovoltaic technology has been industrialized in the existing decades however, it still needs to be upgraded to attain the utmost output (Yaqoob et al., 2021). Usually, 173,000 terawatts of solar energy is received by the earth's surface which is 10,000 times greater than the overall energy consumption (Aboulouard et al., 2021). The energy generated by PV cells epitomizes around 1% of the total energy requirement. It turns out that the required electrical power can be domestically produced by decreasing electrical deficits as well as storage capacities (Traverse et al., 2017).

Based on the material and techniques utilized to engineer solar cells, the PV cells are categorized into three generations. Initially, silicon based first-generation solar cells were developed and these cells were used for a long duration due to their stability, heat constancy and high efficiency. Later on, second and third-generation thin-film PV cells were introduced to overcome the deficiencies of crystalline silicon photovoltaics *i.e.*, high cost of production and problematic installation on large scale (Conibeer et al., 2008; Green, 2004; Heidarzadeh and Tavousi, 2019). Over the last 15 years, apparent improvements in 'second generation' thin-film cells have been made. With the use of thin film, the cost of the material has been reduced by eradicating silicon. Furthermore, power conversion efficiency (PCE) has been significantly improved. With the passage of time as technology advanced, the manufacturing cost has dominated over the cost of material (Green, 2002). Thus, further progress of thin-film photovoltaics (PVs) confronted bottlenecks and the research on third-generation PVs has been progressed. These cells do not contain p-n junction as in conventional solar cells (Arjunan and Senthil, 2013) and are suitable for large-scale installation of PVs (Conibeer, 2007). Third-generation PV cells include polymer, organic PVs, (Yan and Saunders, 2014) hot carrier solar cells, (Tavousi, 2019) multi-junction cells (Conibeer, 2007) etc.

A keen examination reveals that OSCs have the potential to be engineered at less cost, effective using simple synthetic route with lightweight and high flexibility (Chen et al., 2011; Mahmood et al., 2018; Zhan and Marder, 2019). Besides, the OSCs exhibit irregular absorption that can be supervised to transmit visible, infrared and ultraviolet light simultaneously (Aboulouard et al., 2021). The active layer in OSCs generally comprises a blend of electron acceptor and donor with a bulk heterojunction (BHJ) structure that facilitates charge separation and transfer of hole and electron to their respective electrodes (Zhan and Marder, 2019). During the last two decades, fullerene derivatives remained the most extensively used acceptors in OSCs as they embrace fascinating assets comprising high PCE and exclusive electron and hole mobility (Yu et al., 1995). However, their morphological instability and confined variability of optoelectronic properties limit the viable progress of this field, particularly restraining the upper attainable device efficacies (Zhan and Marder, 2019). Organic fullerene-free acceptors offer the probability to overcome these limitations. Less toxicity, facile synthesis, lower level of highest occupied molecular orbital (HOMO) and fine absorption spectrum made non-fullerene acceptors (NFAs) progress a mainstream of today's research (Chan et al., 2017; Sun et al., 2018). Moreover, NFAs having acceptor–donor-acceptor (A-D-A) backbone presented around 17% PCE (Lin et al., 2019). They substantially enrich the carrier mobility with high intramolecular charge transfer rate within a molecule (Firdaus et al., 2020; Xu et al., 2019).

End-group modulation is viewed as an effective approach to modulate the optoelectronic behavior of materials utilized in PV devices (Khan et al., 2021a, 2021b, 2020). Herein, keeping in view the crystallinity and remarkable PCE of indacenodithiophene (IDT) (Arshad et al., 2022), we utilized it as π-spacer and enlarged π-conjugation with 1-phenyl-4,5-dihydro-1H-pyrazole. The **THP1** derivative is developed by attaching 3-ethylidenepentanedinitrile as end-capped acceptor moiety with π-spacer. The remaining chromophores (**THP2-THP8**) are designed by amending terminal acceptor entities (Szukalski et al., 2017). A comprehensive DFT study of designed derivatives (**THP1-THP8**) is performed with the characterization of essential parameters like the frontier molecular orbital (FMO), density of state (DOS), global reactivity parameters (GRPs), transition density matrix (TDM), reorganization energy and open circuit voltage (V_{oc}) to explore the PV response of afore-said compounds. It is estimated that these innovative NFAs would play an indispensable role in the engineering of highly proficient OSCs.

2. Computational study

In the current investigation, non-fullerene electron acceptors having ladder-like backbone were designed by structural modulation of several end-capped acceptors. Gaussian 09 program package (Frisch et al., 2009) was utilized to compute the entire theoretical calculations of the studied chromophores (**THP1-THP8**). The optimization of **THP1-THP8** was accomplished by using Minnesota 06 (M06) (Bryantsev et al., 2009) exchange-correlational functional along with 6-311G(d,p) (Andersson and Uvdal, 2005) basis set. Furthermore, to visualize the photovoltaic and optoelectronic properties, FMO, GRPs, DOS, V_{oc}, UV–Vis absorption and TDM analyses were accomplished at the TD-DFT/M06/6-311G(d,p) level. A number of software *i.e.*, Avogadro, (Hanwell et al., 2012) Gaussum, (O'boyle et al., 2008) Chemcraft, (Zhurko and Zhurko, 2009) PyMOlyze 2.0, (UrRehman et al., 2022) Multiwfn 3.7 (Lu and Chen, 2012) and Gauss view 6.0 (Dennington et al., 2016) were utilized to elucidate the results from output files.

Usually, reorganization energy is utilized to study the rate of charge transference and is segregated into two main types *i.e.*, internal reorganization energy (λ_{int}) and external reorganization energies (λ_{ext}). λ_{int} is concerned with the quick variations in internal composition, while λ_{ext} is directly linked with the external environmental relaxation (Janjua, 2012; Khalid et al., 2020b). In this work, λ_{ext} effect was neglected because of the little contribution of external environmental factors, so λ_{int} was considered. Hence, the reorganization

energy of hole (λ_h) and electron (λ_e) can be computed with the aid of Eqs. (1) and (2) (Mehboob et al., 2021b).

$$\lambda_e = \left[E_0^- - E_-\right] + \left[E_-^0 - E_0\right] \quad (1)$$

$$\lambda_h = \left[E_0^+ - E_+\right] + \left[E_+^0 - E_0\right] \quad (2)$$

where, E_0^+ and E_0^- are the cationic and anionic energies acquired through optimized neutral molecular structure, whereas E_+^0 and E_-^0 are energies of neutral molecule evaluated at cationic and anionic state, respectively. E_- and E_+ specify the energies of optimized anionic and cationic structures, correspondingly. E_0 epitomizes single energy at the ground state (Tang and Zhang, 2012).

3. Results and discussion

The present quantum chemical research envisages some effective NFAs having A-π-A framework with pyrazoline ring as a crucial component of each structure, are signified in Figure S1 and the optimized structures are illustrated in Fig. 2. In this report, eight novel molecules (Figure S1) are designed utilizing the end-capped modification approach to further discover the potential of IDT related compounds. The IUPAC names of compounds are given in Table S9 and structures of all the acceptors that are utilized in structural modulation are shown in Figure S2. Furthermore, their Cartesian coordinates are presented in Tables S1-S8. Literature survey discloses that acceptor groups are essential in tuning the absorption wavelength as well as energy gap of a compound (Khan et al., 2018). Thus, eight derivatives (**THP1-THP8**) are being designed by changing acceptor moieties to discover and enhance the electronic properties of OSCs. Moreover, to analyze how various acceptors affect the PV and spectral response, several parameters such as UV–Vis absorption wavelength, V_{oc} and GRP have been computed by TD-DFT and DFT calculations. The schematic demonstration of **THP1-THP8** are presented in Fig. 1.

3.1. Frontier molecular orbital (FMO) analysis

FMO analysis is an effective approach for exploring the optoelectronic characteristics and chemical stability of the molecule (Javed et al., 2014). The mechanical modeling and absorption spectrum are greatly influenced by FMOs *i.e.*, HOMO and LUMO considered as valence and conduction bands, respectively (Mandado et al., 2006). This analysis unveils the electronic distribution pattern and also provide information about the properties of PVs having the capability to accelerate the transmission of electric current (Khan et al., 2019c; Peng and Yu, 1994). The energy gap among FMOs ($\Delta E = E_{LUMO}$-E_{HOMO}) is believed as a hallmark of aptitude to transfer charge (Janjua et al., 2012b, 2012a; Khan et al., 2019b). The conjugation within the molecule enhances the carrier mobility of the designed molecular system owing to the electronic transitions (Mustafa et al., 2023). Energies of HOMO/LUMO and their band gaps are entirely coupled with the PCE of OSCs (Shafiq et al., 2023a). It also depicts the chemical hardness, softness, molecular interactions and reactivity within the compounds (Amiri et al., 2016). FMO analysis was executed at TD-DFT/M06/6-311G(d,p) level and the calculated energies as well as their E_{gap} are demonstrated in Table 1. Furthermore, the pictographic illustration of key orbitals is presented in Fig. 3 while the other molecular orbitals (HOMO-1/LUMO + 1 and HOMO-2/LUMO + 2) are displayed in Figure S3 and their relevant E_{gap} is tabulated Table S10.

From literature, it has been noticed that experimentally determined HOMO/LUMO values (-5.63/-3.86 *eV*) of **IDIC-C8** compound (Zhang et al., 2020) shows harmonization with the DFT computed results of our designed chromophores. The theoretically calculated E_{HOMO} values of **THP1-THP8** are −5.525, −5.381, −5.111, −5.080, −4.921, −5.349–5.180 and −5.009 *eV*, correspondingly while their E_{LUMO} values are −3.018, −3.017, −2.691, −2.368, −2.190, −2.846, −2.577 and −2.128 *eV*, respectively. The E_{gap} of **THP1-THP8** is observed as 2.507, 2.364, 2.420, 2.712, 2.731, 2.503, 2.603

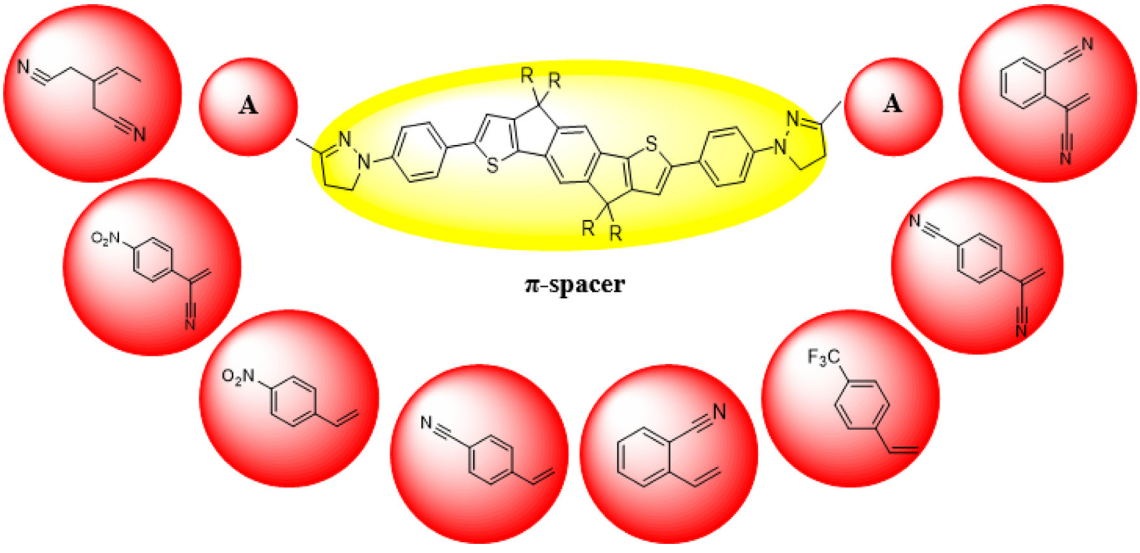

Fig. 1 Schematic illustration of the designed compounds.

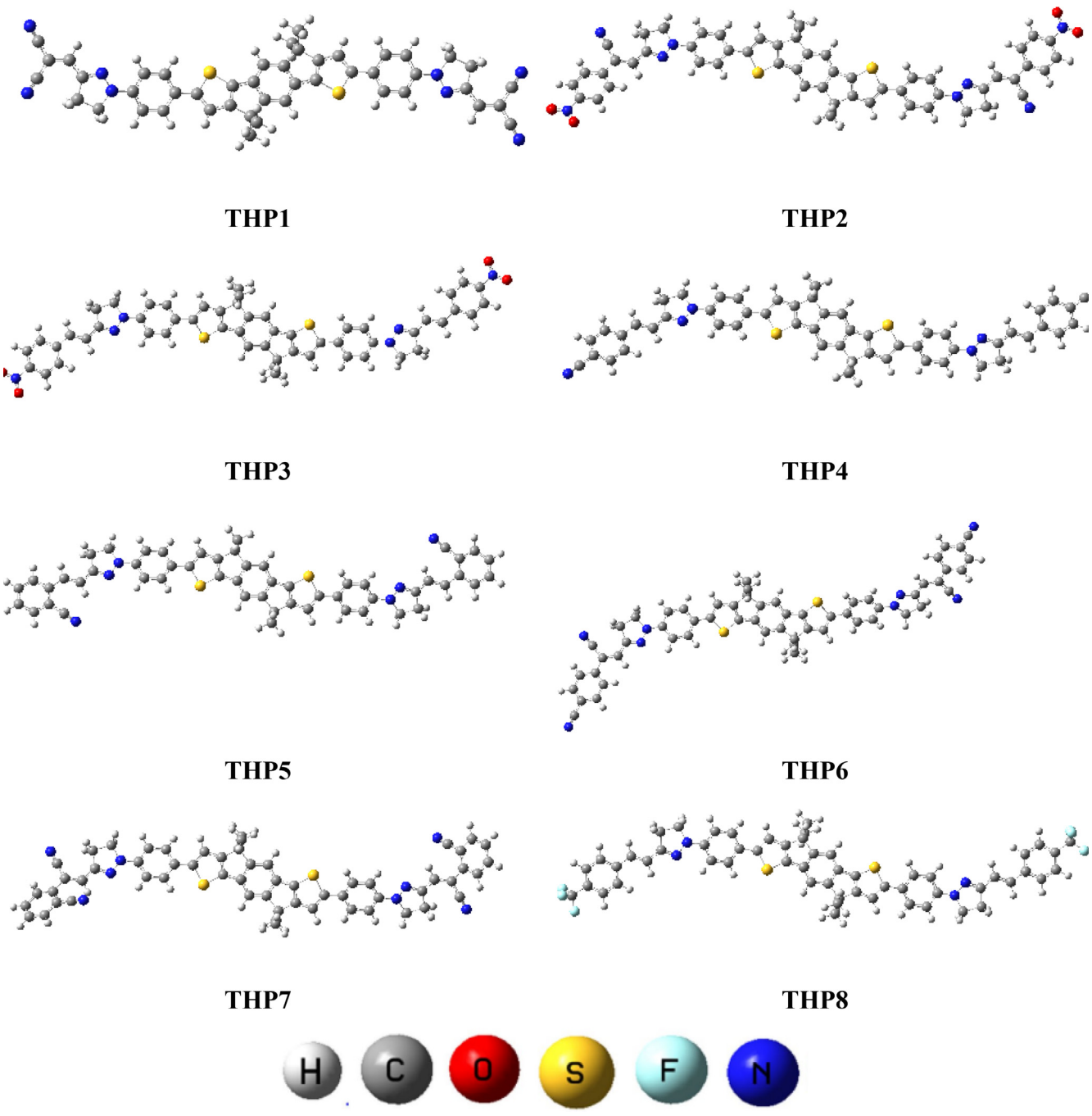

Fig. 2 Optimized structures of all the theoretically computed molecules (**THP1-THP8**).

and 2.881 *eV*, respectively. The maximum value of E_{gap} is noticed in **THP8** (having three fluoro groups at terminal acceptor) *i.e.,* 2.881 *eV* which is the uppermost value among all the derivatives (**THP1-THP8**). The fluorine substituents have lowest electron withdrawing capability than nitro and cyano groups utilized in other chromophores which resulted in superior E_{gap} of **THP8**. The E_{gap} value is declined to 2.712 and 2.731 *eV* in **THP4** and **THP5**, respectively owing to the cyano group at para and ortho positions of peripheral acceptor unit (2-vinylbenzonitrile). In **THP7** and **THP6**, the E_{gap} is further dropped to 2.603 and 2.503 *eV* due to the 2-(1-cyanovinyl) benzonitrile and 4-(1-cyanovinyl) benzonitrile end-capped groups. Moreover, the E_{gap} of 2.507 *eV* is noticed in **THP1** that might be due to the existence of two cyano groups at the terminal acceptors. The greater electronegativity of cyano groups increases the acceptors capability to pull the electrons towards itself, results in reduced E_{gap} among orbitals. Remarkably, the HOMO and LUMO energy difference is lowered to 2.420 *eV* in **THP3** due to the presence of sole nitro group which has greater electron withdrawing capability. Moreover, the smallest value (2.364 *eV*) of E_{gap} is viewed in **THP2** owing to the nitro group which has strong electron withdrawing (*-I*) nature that attracts the electron density towards itself. Further, the presence of cyano group in the vicinity of benzene ring also

Table 1 E_{HOMO}, E_{LUMO}, and energy gap (E_{gap} = E_{LUMO}-E_{HOMO}) of the **THP1-THP8**.

Compounds	HOMO	LUMO	E_{gap}
THP1	−5.525	−3.018	2.507
THP2	−5.381	−3.017	2.364
THP3	−5.111	−2.691	2.420
THP4	−5.080	−2.368	2.712
THP5	−4.921	−2.190	2.731
THP6	−5.349	−2.846	2.503
THP7	−5.180	−2.577	2.603
THP8	−5.009	−2.128	2.881

Units in *eV*.

abridged the E_{gap}. Moreover, the overall decreasing trend of E_{gap} is as follows: **THP8 > THP5 > THP4 > THP7 > THP1 > THP6 > THP3 > THP2**. The effective charge mobility and lowest E_{gap} between orbitals is inspected in **THP2** than all the examined chromophore that emerged as a competent PV-material.

The scheme of electronic charge distribution over the surface areas of **THP1-THP8** is illustrated in Fig. 3. The electronic cloud is majorly occupied on π-spacer in HOMO, while in LUMO it is mainly concentrated on over terminal acceptors and minutely over π-spacer. This designates that substantial assistance of charge transmission from π-spacer towards acceptors is monitored in all the designed compounds (**THP1-THP8**).

3.2. Density of state (DOS)

The DOS investigation was performed at M06 functional with 6-311G basis set to interpret the findings of **THP1-THP7**. To envisage the path of charge transmission, we separated our investigated chromophores into two fragments *i.e.*, acceptor and π-spacer that are portrayed by green and red lines, correspondingly as shown in Fig. 4. The DOS study has been executed to ascertain the valuable contribution of every fragment over the molecular system which has particular number of electronic states (Adeel et al., 2021). It has unveiled the charge dissemination from HOMO which has large capacity to donate electrons to LUMO that has tendency to accept electrons (Goszczycki et al., 2017). The pattern of charge dissemination is changed by varying acceptor units that is supported by HOMO/LUMO percentage of DOS (Table S11). Herein, acceptor demonstrates the contribution of electronic charges as: 4.5, 5.5, 5.0, 5.1, 5.0, 5.6, 5.1 and 5.0% to HOMO, while 52.2, 70.4, 81.7, 68.2, 69.2, 62.4, 60.2 and 61.2% to LUMO for **THP1-THP8**, correspondingly. Similarly, π-spacer reveals the distribution of charges as: 95.5, 94.5, 95.0, 94.9, 95.0, 94.4, 94.9 and 95.0% to HOMO, whereas 47.8, 29.6, 18.3,

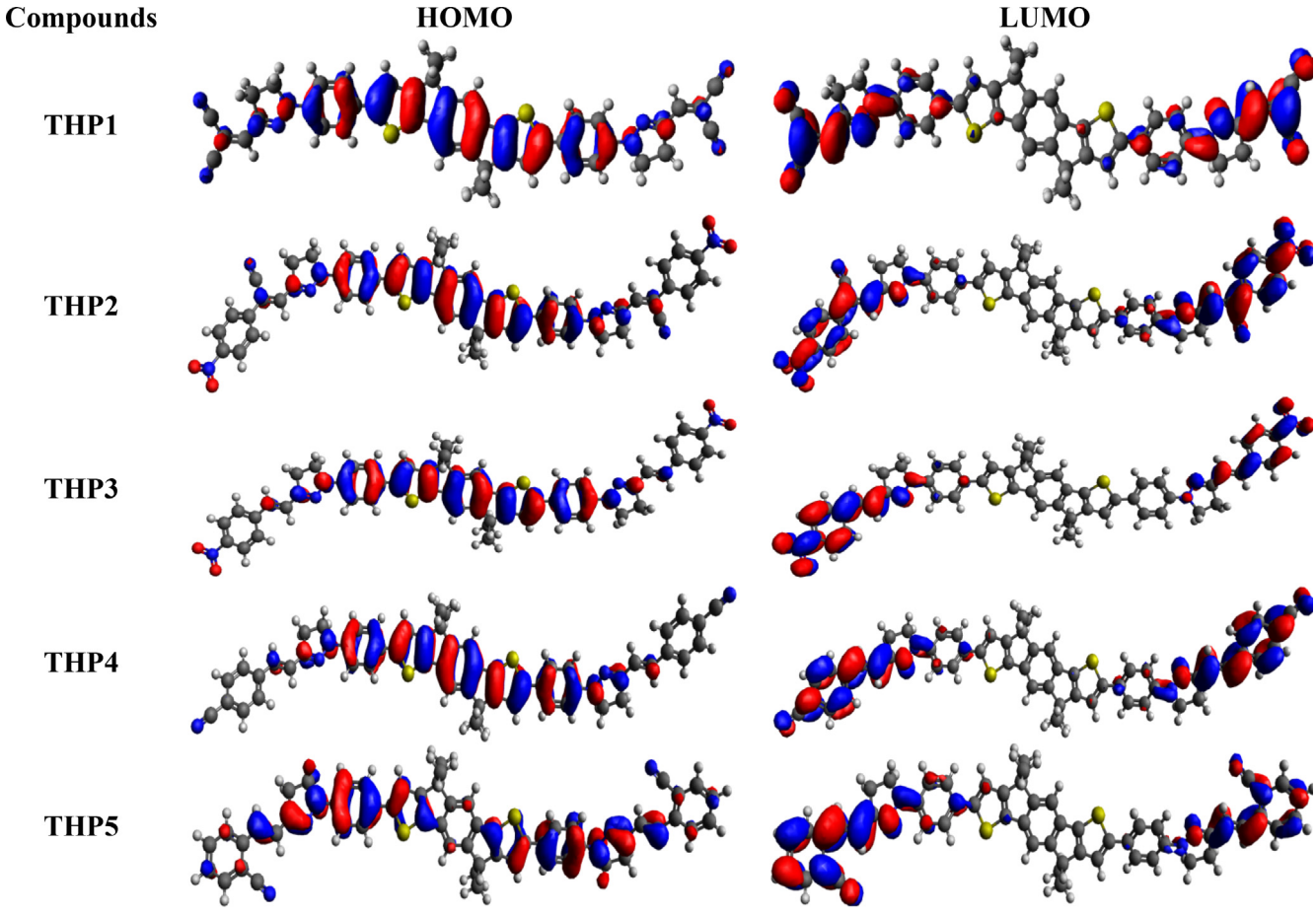

Fig. 3 The FMOs (HOMO and LUMO) of **THP1-THP8**.

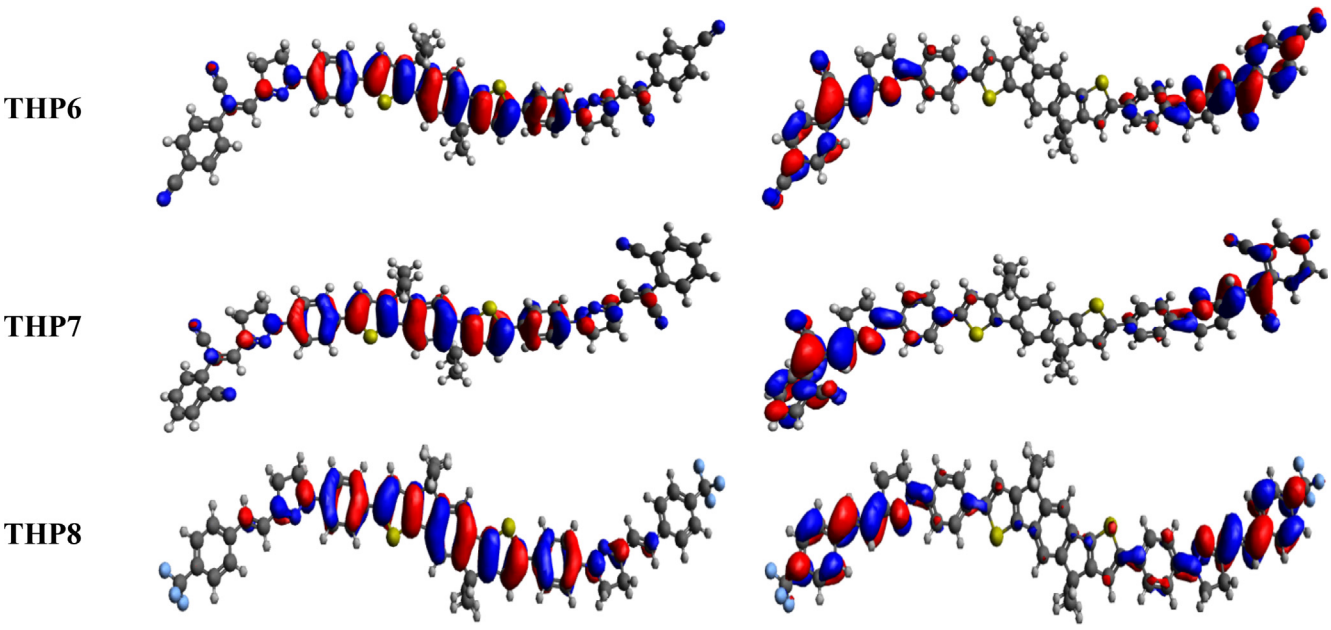

Fig. 3 (*continued*)

31.8, 30.7, 37.6, 39.8 and 38.8% to LUMO for **THP1-THP8**, respectively. In DOS graphs, the negative values denote the HOMO, whereas the positive values show LUMO along x-axis and the E_{gap} expresses the distance among HOMOs and LUMOs (Khalid et al., 2022c). From DOS spectrum, it is anticipated that maximum charge density of HOMO is positioned over π-spacer at approximately −13 *eV* whereas LUMO is mainly resided over acceptor with highest peak at 3.5 *eV* in the aforesaid compounds. Overall, DOS analysis exhibits extensive charge transfer from π-bridge towards peripheral acceptor moieties in all the studied chromophores.

3.3. Optical response

TD-DFT computations are utilized to investigate the absorption spectrum of the titled chromophores (**THP1-THP8**) in gas phase at M06 with 6-311G(d,p) basis set. UV–Vis analysis gives substantial information about the nature of electronic transitions, possibility of charge transference as well as contributing configuration of the molecule. The oscillator strength (f_{os}), maximum absorption wavelengths (λ_{max}) and excitation energies (E) of lowest six singlet–singlet electronic transitions were examined and the outcomes are tabulated in Tables S13-S20, whereas some main results are depicted in Table S12. The optical absorption spectra of **THP1-THP8** are exhibited in Fig. 5 in gaseous phase. The electronic excitation spectrum of the examined compounds is envisioned to acknowledge the influence of several acceptors on the spectral properties.

The results mentioned in Table S12 has disclosed that all the studied molecules display absorption in the visible region. The simulated λ_{max} of **THP1-THP8** are found in the range of 512.861—584.555 *nm* with oscillation strength of 1.807–2.951 and excitation energy of 2.008–2.417 *eV* in gaseous phase. The compound (**THP2**) depicted highest λ_{max} value of 617.482 *nm* with transition energy value of 2.008 *eV* and 1.948 oscillation strength presenting 93% molecular orbital (MO) contribution from HOMO to LUMO. The utmost value of λ_{max} in **THP2** is ascribed to the extensively electron accepting nitro and cyano groups. The λ_{max} in **THP3** is abridged to 589.166 *nm* owing to 1-nitro-4-vinylbenzene group. In addition, in **THP6**, the λ_{max} value is observed as 588.021 *nm* that is larger than **THP1** and **THP7** (584.555 and 567.096 *nm*, respectively). Furthermore, this value is squeezed to 539.202 and 537.123 *nm* in **THP4** and **THP5** due to the incorporation of cyano groups at the end-capped acceptors. The computed maximum wavelength for **THP8** is observed at 512.861 *nm* with transition energy 2.417 *eV* and oscillation strength as 2.951 which is the lowermost value among all the studied compounds. The values of λ_{max} are noticed in the subsequent declining trend as: **THP2 > THP3 > THP6 > THP1 > THP7 > THP4 > THP5 > THP8**. Lower excitation energy and increase in wavelength disclose that **THP1-THP8** molecules exhibit greater charge transfer aptitude, consequently easy transition might occur amongst HOMO and LUMO. In a nutshell, **THP2** possess highest λ_{max}, least energy gap and minimum transition energy among all the derivatives which might be anticipated as a suitable material for OSCs.

3.4. Global reactivity parameters (GRPs)

The energy gap of HOMO and LUMO is utilized to compute the GRPs (Khalid et al., 2020a) of the entitled compounds (**THP1-THP8**) which in turn determine their reactivity as well as stability. Therefore, E_{gap} is a dynamic feature to evaluate the GRPs such as electron affinity (EA), electronegativity (X), ionization potential (IP), softness (σ), electrophilicity index (ω), hardness (η) and chemical potential (μ) (Sheela et al., 2014). The ionization potential ($IP = -E_{HOMO}$) and electron affinity ($EA = -E_{LUMO}$) are calculated utilizing the given formulas (Pearson, 1986). Koopman's theorem (Koopmans, 1934) is used to calculate the electronegativity [$X = (IP + EA)/2$],

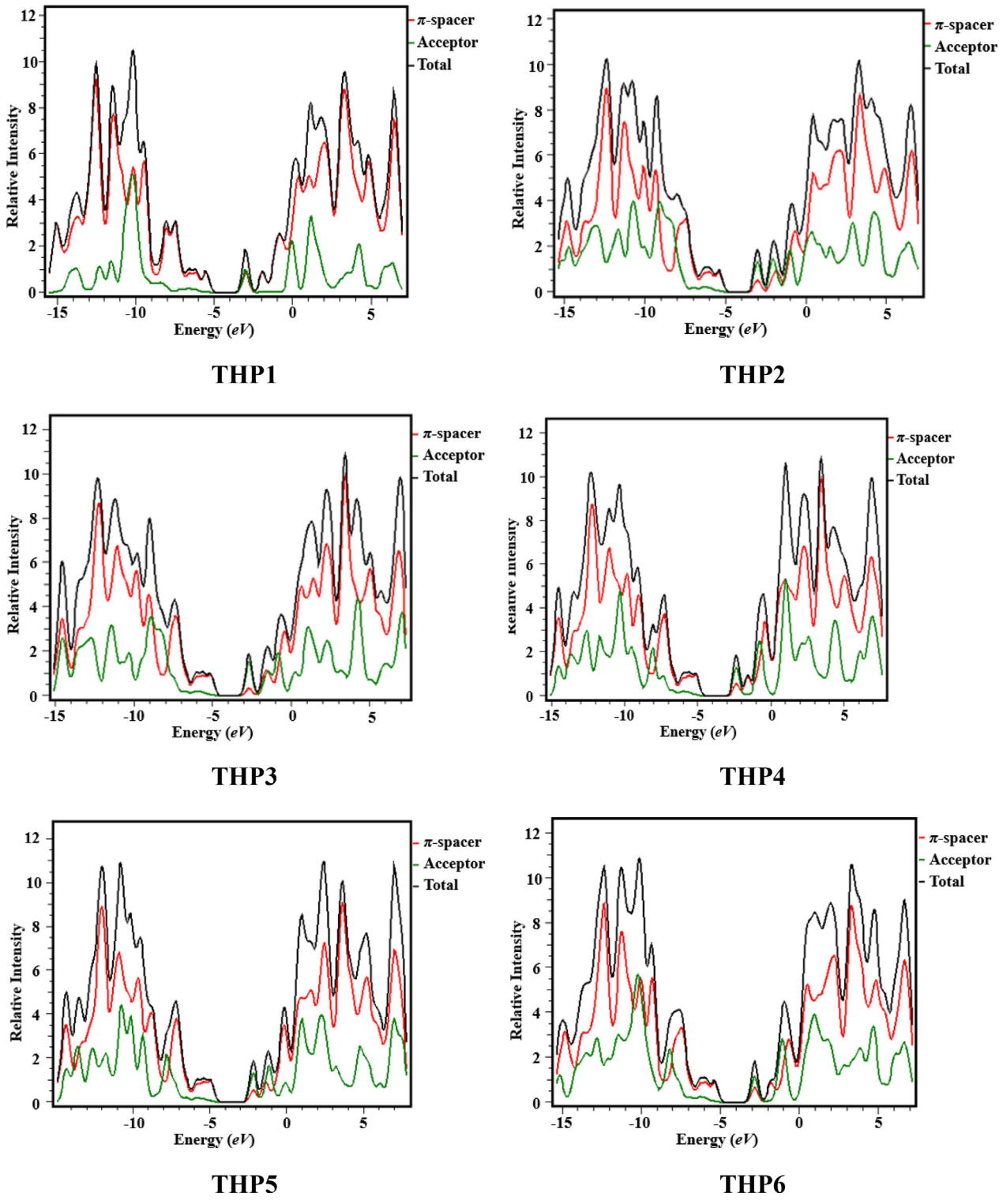

Fig. 4 Graphical illustration of DOS of the titled compounds (**THP1-THP8**).

chemical hardness [$\eta = (IP - EA)/2$] and chemical potential [$\mu = E_{HOMO} + E_{LUMO})/2$]. Parr *et al.* (Parr et al., 1978) described the global electrophilicity index that is computed *via* using the given equation ($\omega = \mu^2/2\eta$) (Chattaraj and Roy, 2007). Moreover, the global softness is determined by the mentioned equation ($\sigma = 1/2\eta$) (Koopmans, 1934). The values of η helps in determining the chemical reactivity and stability, (Pearson, 2005) while μ describes the electronic movement within the molecule (Toro-Labbé, 1999). Further, ω aids in determining the stability of a molecule when an additional

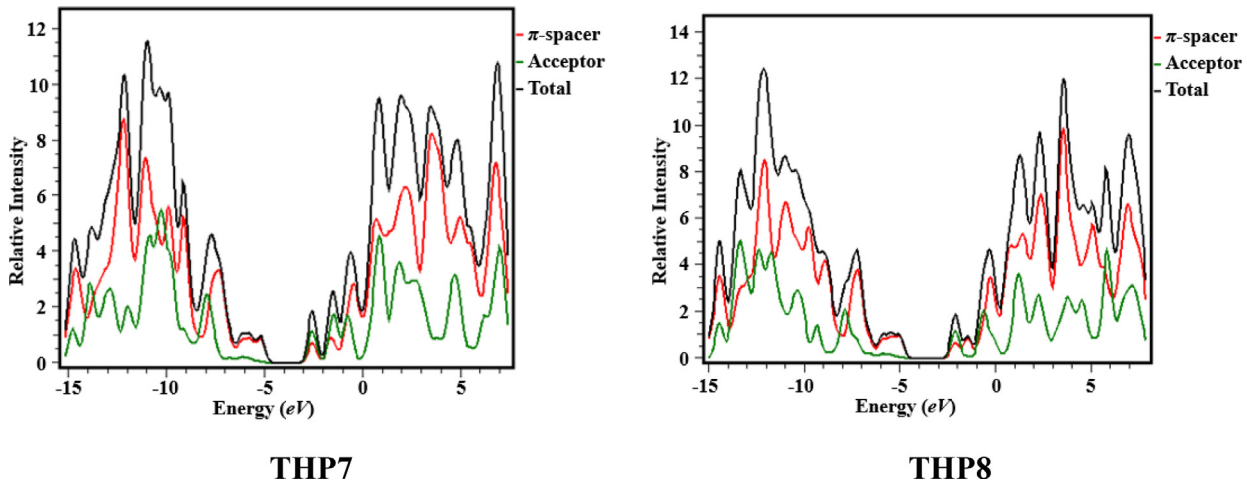

Fig. 4 (*continued*)

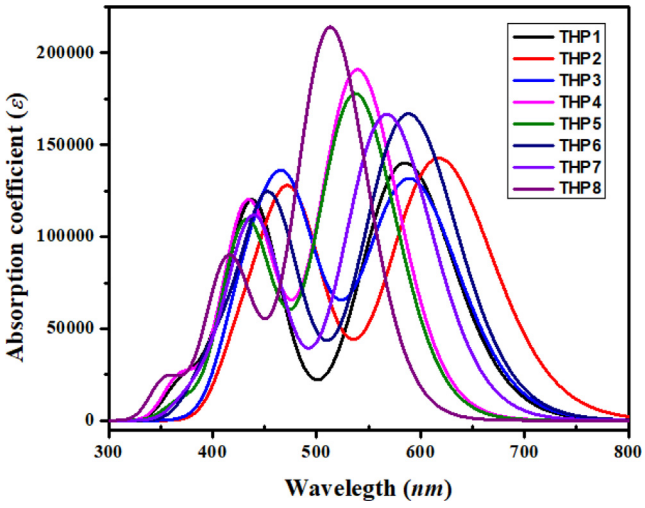

Fig. 5 Absorption spectra of entitled compounds **THP1-THP8**.

electronic charge is acquired by it from an external source (Parr et al., 1999).

Table 2 elucidates the outcomes of GRPs for **THP1-THP8** which are discussed here. The *IP* and *EA* designates the donating and accepting ability of a specie and are identical to the potential needed to transmit an electron from HOMO to LUMO. The polarization of a molecule is in direct relation with the *EA* and *IP*, which discloses the reactivity of a molecule. **THP1-THP8** exhibit the high *IP* values (5.009–5.525 *eV*) and low *EA* values (2.128–3.018 *eV*) as mentioned in Table 2. All the studied molecules manifest comparable *EA* values which endorse their accepting nature. This might be owing to the existence of vigorous acceptors at the terminal portions of molecules. The values of X and ω also upholds the abovementioned statement. The chemical potential, global softness and hardness are correlated with the E_{gap} and also give information about the reactivity. Thus, a compound with less E_{gap} is considered as highly reactivity, soft and less stable. However, the compound with high E_{gap} is assessed to be least reactive, hard and more kinetically stable.(Tahir et al., 2017) The increasing order of softness is: **THP8 < THP5 < THP4 < THP7 < THP1 < THP6 < THP3 < THP2** with values as: 0.347 < 0.3662 < 0.3687 < 0.384 < 0.398 < 0.400 < 0.413 < 0.423 *eV*. Interestingly, **THP2** exhibit the highest softness value that made it more polarized as well as reactive chromophore which might holds probable PV aptitude.

3.5. Reorganization energy

Reorganization energy (λ) analysis is another essential tool utilized to disclose the performance and working of OSCs. Generally, λ is inversely correlated with the charge mobilities (hole and electron) (Köse et al., 2007). The lesser the reorganization energy, the greater will be the carrier mobility of a molecule. Reorganization energy is fluctuated by altering particular conditions, but these variations majorly influenced by the cationic and anionic geometries. Anionic geometry epitomizes electron

Table 2 GRP values of the studied chromophores (**THP1-THP8**) in *eV*.

Compounds	*IP*	*EA*	*X*	*η*	*μ*	*ω*	*σ*
THP1	5.525	3.018	4.271	1.253	−4.271	7.277	0.398
THP2	5.381	3.017	4.199	1.182	−4.199	7.458	0.423
THP3	5.111	2.691	3.901	1.210	−3.901	6.288	0.413
THP4	5.080	2.368	3.724	1.356	−3.724	5.113	0.368
THP5	4.921	2.190	3.555	1.365	−3.555	4.629	0.366
THP6	5.349	2.846	4.097	1.251	−4.097	6.708	0.400
THP7	5.180	2.577	3.878	1.301	−3.878	5.779	0.384
THP8	5.009	2.128	3.568	1.440	−3.568	4.420	0.347

transferal from the donor substance, whereas cationic geometry denotes hole transmission from acceptor material (Afzal et al., 2020). Reorganization energy is characterized into λ_{int} and λ_{ext}, but we preferably choose λ_{int} by neglecting λ_{ext}. The values of λ_h and λ_e are computed using Eqs. (1) and (2) and the results are collected in Table 3.

From literature survey, it has been observed that Bary et al., reported **A1-A5** compounds which showed λ_e values in the range of 0.0077–0.0007 eV while λ_h values was found in the range of 0.0403–0.0003 eV (Bary et al., 2021) that are somewhat comparable to our designed compounds. Likewise, Adnan et al., reported that λ_e and λ_h values of **R** and **CS1-CS5** are found in the range of 0.0184–0.0104 eV and 0.0206–0.0163 eV, respectively (Adnan et al., 2021). Kayani et al., observed that compounds **R** and **Rm1-Rm4** depicted λ_e of 0.2290–0.0038 eV whereas λ_h values are noticed in the range of 0.0108–0.0072 eV (Kayani et al., 2021). Furthermore, Mehboob et al., studied **R** and **H1-H5** chromophores which showed λ_e and λ_h values in the range of 0.0088–0.0104 eV and 0.0090–0.0060 eV, correspondingly (Mehboob et al., 2021c). Siddique et al., reported that **R** and **D1-D4** compounds depicted λ_e values in the range of 0.1915–0.1344 eV whereas λ_h values are noticed in the range of 0.0834–0.0629 eV (Siddique et al., 2020) which are overestimated than out entitled compounds. The computed values of electron motilities for **THP1-THP8** are −0.0002, −0.0005, −0.0004, −0.0004, −0.0008, −0.0007, −0.0006, −0.00004 eV, respectively. Among all studied chromophores, **THP5** depicted the lowest value of λ_e which shows greater electron transference rate between HOMO and LUMO. Likewise, **THP6** and **THP2** have significantly better charge mobilities due to their lesser λ_e values. The escalating order of λ_e for the all the entitled compounds is: **THP5 < THP6 < THP2 < THP4 = TH P3 < THP1 < THP8**. Similarly, the theoretically computed λ_h values for **THP1-THP8** are 0.0006, −0.000007, −0.0002, −0.0004, −0.0003, −0.0005, −0.0002, −0.0004 eV, correspondingly. The ascending order of λ_h for all the entitled compounds are: **THP6 < THP4 = THP8 < THP5 < THP3 = THP7 < THP2 < THP1**. This analysis disclosed that λ_e values of all the examined chromophores are observed lower than λ_h values except **THP8**. Overall, the reduction in terms of λ_e designates that all the chromophores are promising applicants for transferal of electrons and can be used as competent PV materials.

Table 3 Computed reorganization energies of **THP1-THP8** chromophores.

Compounds	λ_e	λ_h
THP1	−0.0002	0.0006
THP2	−0.0005	−0.000007
THP3	−0.0004	−0.0002
THP4	−0.0004	−0.0004
THP5	−0.0008	−0.0003
THP6	−0.0007	−0.0005
THP7	−0.0006	−0.0002
THP8	−0.00004	−0.0004

Units in eV.

3.6. Open circuit voltage (V_{oc})

Open Circuit Voltage (V_{oc}) is indispensable to elucidate the performance of OSCs and shows the maximum magnitude of voltage that can be taken out from any optically active material at zero current (Tang and Zhang, 2012). It plays an indispensable role to get insights into the working mechanics of organic semiconductor materials (Irfan et al., 2017). Numerous features influence the V_{oc} *i.e.*, light source, light intensity, temperature of OSCs, external environmental proficiency, charge carrier recombination and several other environmental factors (Saleem et al., 2021). Primarily, V_{oc} is influenced by light generation and saturation voltage that helps in the recombination of PV devices. The E_{gap} of donor and acceptor *i.e.*, $HOMO_{PBDB\text{-}T}$-$LUMO_{acceptor}$ is directly associated with the V_{oc}. In the present quantum chemical calculations, PBDB-T donor molecule (Zheng et al., 2020) (which has E_{HOMO} of −5.401 eV) is used to compute the V_{oc} and the findings are summarized in Fig. 6. The calculated V_{oc} outcomes of **THP1-THP8** by using Eq. (3) developed by Scharber (Scharber et al., 2006) are grouped in Table 4.

$$Voc = (|E^{D}_{HOMO}| - |E^{A}_{LUMO}|) - 0.3 \quad (3)$$

The computed values of V_{oc} of **THP1-THP8** with regards to the energy gap of $HOMO_{donor}$ –$LUMO_{acceptor}$ are examined to be 2.083, 2.084, 2.410, 2.733, 2.911, 2.255, 2.524 and 2.973 V, correspondingly. The V_{oc} of the examined compounds are perceived to be in the subsequent declining order: **THP8 > THP5 > THP4 > THP7 > THP3 > THP6 > THP2 > THP1**. The highest value of V_{oc} is noticed in **THP8** at 2.973 V and this larger V_{oc} value demonstrates the contribu-

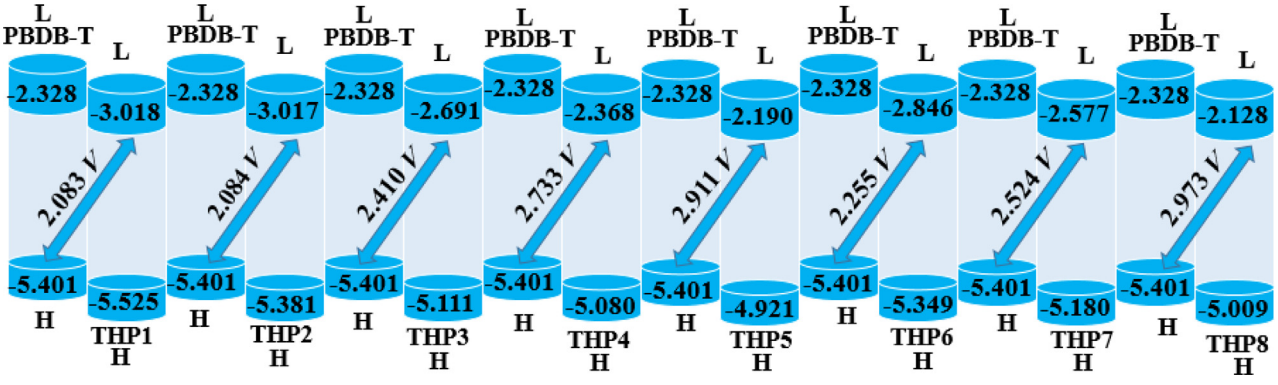

Fig. 6 Diagrammatic representation of V_{oc} of **THP1-THP8** with **PBDB-T**.

Table 4 V_{oc} of the entitled compounds (**THP1-THP8**). $\Delta E = E^{A}_{LUMO} - E^{D}_{HOMO}$.

Compounds	V_{OC} (V)	Δ E (eV)
THP1	2.083	2.383
THP2	2.084	2.384
THP3	2.410	2.71
THP4	2.733	3.033
THP5	2.911	3.211
THP6	2.255	2.555
THP7	2.524	2.824
THP8	2.973	3.273

tion to their superior LUMO values. Moreover, the V_{oc} values majorly depends on the energy difference of a molecule that is an innate property of semiconductors. Having less energy gap means relaxed excitation and maximum photons would have greater energy than required for excitation producing more electricity with greater PV response and higher PCE. In this report, we made BHJ device by blending PBDB-T donor polymer with our designed acceptor molecules. When the complex developed, we observed that low level of LUMO of our acceptors enhance the transfer of charge carriers from HOMO of PBDB-T and thus escalate the transitions which results in higher efficiencies.

3.7. Transition density matrix (TDM)

TDM analysis assists in interpreting the transition process, (Ans et al., 2019) electronic excitation state and hole-electron overlapping (Mehboob et al., 2021a). In addition, it is very valuable in evaluating the behavior of electronic transitions in the excited (S_1) state, interaction among acceptor and donor entities accompanied by electron and hole localization as well as the extent of intramolecular charge transference (Ans et al., 2018). The determination of these parameters aids in evaluating the function of OSCs. M06 method in conjunction with 6-311G(d,p) basis set was used to ascertain the absorption

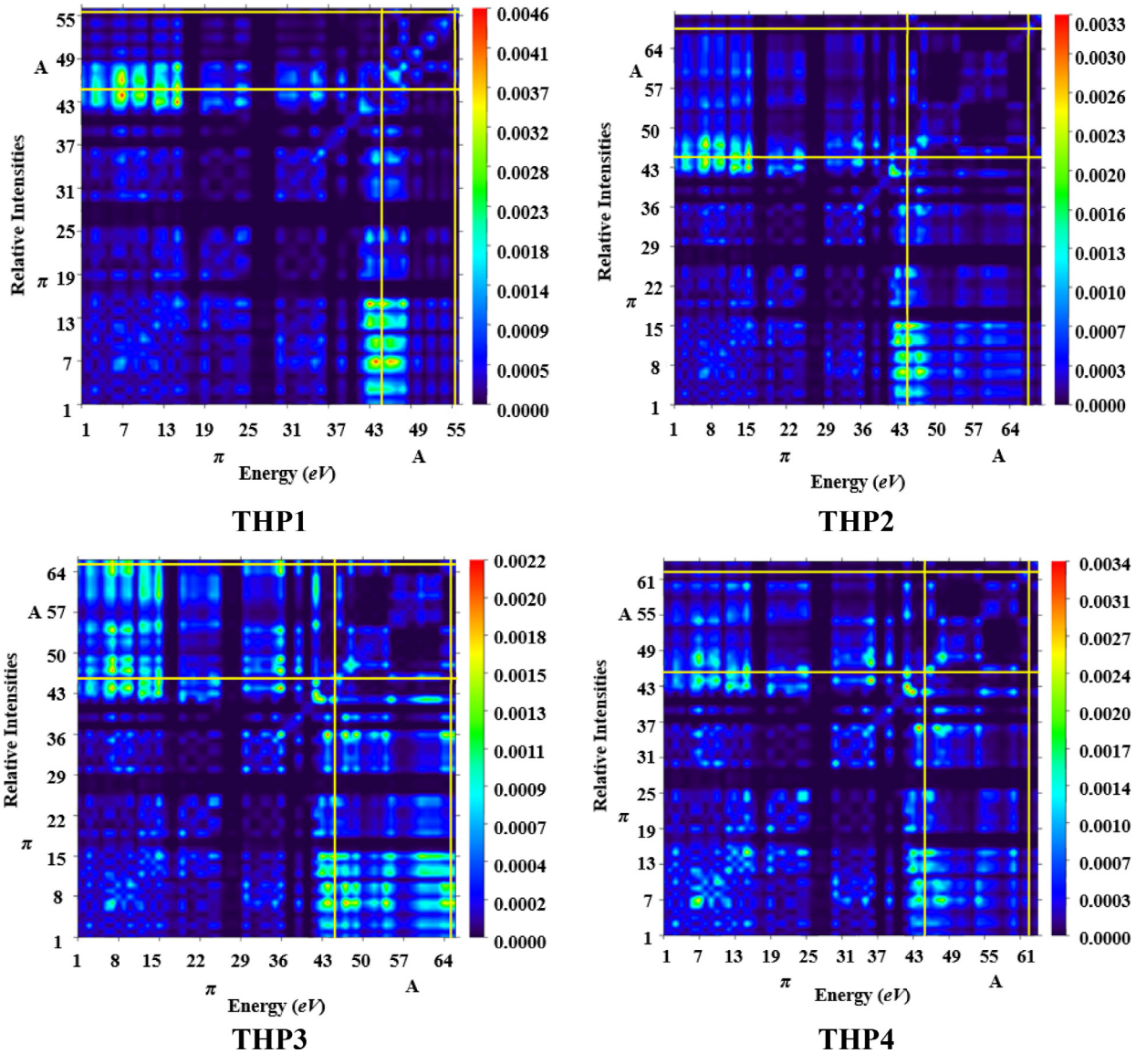

Fig. 7 TDM graphs of the titled molecules (**THP1-THP8**).

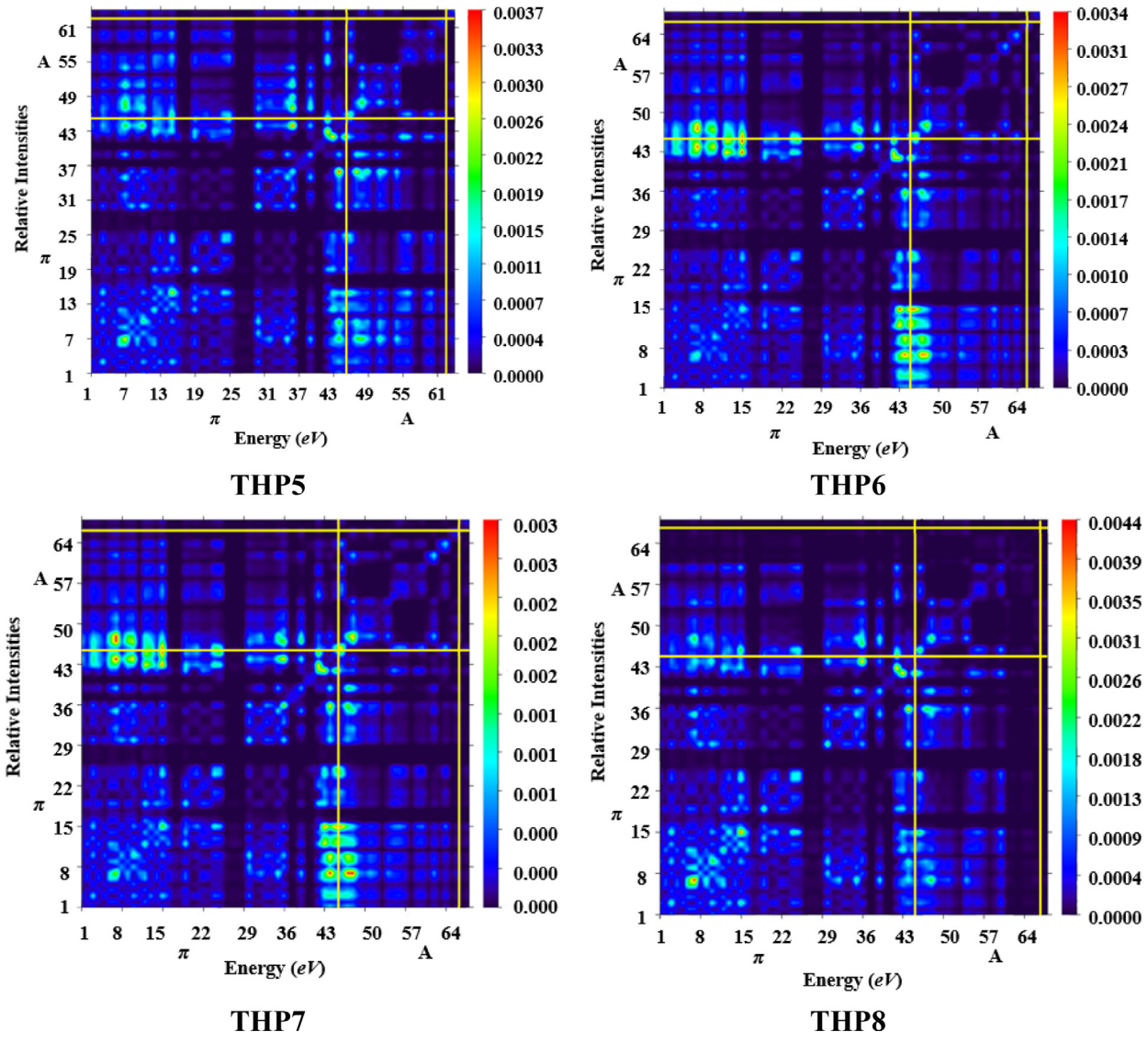

Fig. 7 (*continued*)

Table 5 Computed $E_{L\text{-}H}$ and E_{opt} of **THP1-THP8**, units are in *eV*.

Compounds	$E_{H\text{-}L}$	E_{opt}	E_b
THP1	2.507	2.121	0.386
THP2	2.364	2.008	0.356
THP3	2.420	2.104	0.316
THP4	2.712	2.299	0.413
THP5	2.731	2.308	0.423
THP6	2.503	2.109	0.394
THP7	2.603	2.186	0.417
THP8	2.881	2.417	0.464

and emission of all the designed chromophores (**THP1-THP8**). This analysis offers a 3D heat map with appropriate color discrepancy *i.e.*, exhibited by blue region. The impact of hydrogen atoms has been overlooked due to their minute contribution in transition. The pictorial display of TDM analysis is given in Fig. 7.

In the current examination, we split our molecules (**THP1-THP8**) into two different portions *i.e.*, acceptor and π-spacer. From FMO investigation, it is revealed that charge transmission is substantially executed over the molecule. The TDM pictographs disclosed that, there is an effective diagonal transmission of electron density from π-spacer towards terminal acceptors in all the chromophores, permitting good charge transference without any confinement. Moreover, electron hole pair generation and excitation of charge coherence also appear to proliferate non-diagonally over the TDM plots. Besides, calculation of TDM maps of **THP1-THP8** indicate schematic, simpler and progressive exciton dissociation in the S_1 state which proves valuable for future applications.

3.8. Exciton binding energy (E_b)

Binding energy (E_b) is another distinctive feature correlated to TDMs that is utilized to evaluate the PV response of OSCs. It is a significant parameter for the evaluation of exciton dissociation capability and columbic force of interaction among elec-

tron and hole. The E_b is in inverse relation to the exciton dissociation and directly associated with columbic interaction (Farhat et al., 2020; Khalid et al., 2022b). The E_b of **THP1-THP8** is computed from the difference in E_{gap} of LUMO-HOMO and optimization energy (E_{opt}) as shown by Eq. (4) (Köse, 2012).

$$E_b = E_{L-H} - E_{opt} \quad (4)$$

In Eq. (4), $E_{L\text{-}H}$ indicates the energy difference among HOMO/LUMO and E_{opt} represents the lowest amount of energy necessary for excitation form S_0 to S_1 state, which generates an electron-hole pair (Janjua et al., 2012b; Khan et al., 2019a). The calculated outcomes of E_b are grouped in Table 5.

The values of E_b for **THP1-THP8** are calculated as 0.386, 0.356, 0.316, 0.413, 0.423, 0.394, 0.417 and 0.464 *eV*, correspondingly. **THP3** gives the lowermost value (0.316 *eV*) of E_b exhibiting higher efficiency of charge dissociation in S_1 state as compared to the other chromophores. Generally, the compounds having 1.9 *eV* or lesser E_b value are regarded as effective PV candidates with inspiring V_{oc}. Remarkably, our titled molecules (**THP1-THP8**) has expressed lower values of E_b than 1.9 *eV*. The descending trend of E_b is: **THP8 > THP5 > THP7 > THP4 > THP6 > THP1 > THP2 > THP3**. So, **THP3** molecule possessed lowest E_b elucidating greatest potential of charge separation with exceptional optical and electronic properties.

4. Conclusion

Conclusively, state-of-the-art quantum chemical procedures have been utilized to inspect the electronic and photophysical capabilities of eight pyrazoline-based NFAs (**THP1-THP8**), designed by altering terminal acceptor moieties. The structural tailoring has demonstrated as a significant strategy to acquire inspiring PV compounds with remarkable optoelectronic possessions for OSCs. FMO study depicted that least band gap of 2.364 *eV* is perceived in **THP2**, while for all the derivatives, E_{gap} values fall in the following range of 2.507–2.881 *eV* with effective charge transference rate that is further endorsed by the DOS and TDM analyses. Furthermore, GRPs studies disclosed that extensive conjugation gives exceptional stability to the studied chromophores. Likewise, **THP1-THP8** displayed red shifted absorption spectra at 512.861–584.555 *nm* range in gas phase. The V_{oc} of **THP1-THP8** with regards to $HOMO_{PBDB\text{-}T}$-$LUMO_{acceptor}$ are observed with satisfactory values. The binding energy of the entitled chromophores (**THP1-THP8**) are found comparable with each other resulted in higher exciton dissociation. Furthermore, least reorganization energy in the above-mentioned chromophores for electron with hole is also examined. Amongst all the designed chromophores, **THP2** owing to the strong electron accepting capability is recognized as a significant candidate for OSCs applications with outstanding PV properties comprising highest λ_{max} (617.482 *nm*), lowest energy gap (2.364 *eV*) and highest softness (0.423 *eV*). Our outcomes indicated that incorporating electron-accepting groups is an effective strategy for designing promising NF based OSCs. The designed molecules specifically **THP2** is suggested for production of high-performance OSCs devices.

Declaration of Competing Interest

The authors declare that they have no known competing financial interests or personal relationships that could have appeared to influence the work reported in this paper.

Acknowledgment

Dr. Muhammad Khalid gratefully acknowledges the financial support of HEC Pakistan (project no. 20-14703/NRPU/R&D/HEC/2021). A. A.C.B. acknowledges the financial support of the Sąo Paulo Research Foundation (FAPESP) (Grants 2014/25770-6 and 2015/01491-3), the Conselho Nacional de Desenvolvimento Científico e Tecnológico (CNPq) of Brazil for academic sup- port (Grant 309715/2017-2), and Coordenac¸ąo de Aperfeic¸oa- mento de Pessoal de Nível Superior – Brasil (CAPES) that partially supported this work (Finance Code 001). The authors thank the Researchers Supporting Project number (RSP2023R6), King Saud University, Riyadh, Saudi Arabia. S.C.O. acknowledges the support from the doctoral research fund of the Affiliated Hospital of Southwest Medical University.

Appendix A. Supplementary material

Supplementary data to this article can be found online at https://doi.org/10.1016/j.arabjc.2023.105271.

References

Aboulouard, A., Mtougui, S., Demir, N., Moubarik, A., Can, M., 2021. New non-fullerene electron acceptors-based on quinoxaline derivatives for organic photovoltaic cells: DFT computational study. Synth. Met. 279, 116846.

Adeel, M., Khalid, M., Ullah, M.A., Muhammad, S., Khan, M.U., Tahir, M.N., Khan, I., Asghar, M., Mughal, K.S., 2021. Exploration of CH··· F & CF··· H mediated supramolecular arrangements into fluorinated terphenyls and theoretical prediction of their third-order nonlinear optical response. RSC Adv. 11, 7766–7778.

Adnan, M., Mehboob, M.Y., Hussain, R., Irshad, Z., 2021. In silico designing of efficient C-shape non-fullerene acceptor molecules having quinoid structure with remarkable photovoltaic properties for high-performance organic solar cells. Optik 241, 166839.

Afzal, Z., Hussain, R., Khan, M.U., Khalid, M., Iqbal, J., Alvi, M.U., Adnan, M., Ahmed, M., Mehboob, M.Y., Hussain, M., 2020. Designing indenothiophene-based acceptor materials with efficient photovoltaic parameters for fullerene-free organic solar cells. J. Mol. Model. 26, 1–17.

Amiri, S.S., Makarem, S., Ahmar, H., Ashenagar, S., 2016. Theoretical studies and spectroscopic characterization of novel 4-methyl-5-((5-phenyl-1, 3, 4-oxadiazol-2-yl) thio) benzene-1, 2-diol. J. Mol. Struct. 1119, 18–24.

Andersson, M.P., Uvdal, P., 2005. New scale factors for harmonic vibrational frequencies using the B3LYP density functional method with the triple-ζ basis set 6–311 + G (d, p). Chem. A Eur. J. 109, 2937–2941.

Ans, M., Iqbal, J., Ahmad, Z., Muhammad, S., Hussain, R., Eliasson, B., Ayub, K., 2018. Designing three-dimensional (3D) non-fullerene small molecule acceptors with efficient photovoltaic parameters. ChemistrySelect 3, 12797–12804.

Ans, M., Ayub, K., Bhatti, I.A., Iqbal, J., 2019. Designing indacenodithiophene based non-fullerene acceptors with a donor–acceptor combined bridge for organic solar cells. RSC Adv. 9, 3605–3617.

Arjunan, T., Senthil, T.S., 2013. Dye sensitised solar cells. Mater. Technol. 28, 9–14.

Arshad, M.N., Shafiq, I., Khalid, M., Asiri, A.M., 2022. Exploration of the intriguing photovoltaic behavior for fused indacenodithio-

phene-based A-D–A conjugated systems: a DFT model study. ACS Omega 7, 11606–11617.
Bary, G., Ghani, L., Jamil, M.I., Arslan, M., Ahmed, W., Ahmad, A., Sajid, M., Ahmad, R., Huang, D., 2021. Designing small organic non-fullerene acceptor molecules with diflorobenzene or quinoline core and dithiophene donor moiety through density functional theory. Sci. Rep. 11, 19683.
Bryantsev, V.S., Diallo, M.S., Van Duin, A.C., Goddard III, W.A., 2009. Evaluation of B3LYP, X3LYP, and M06-class density functionals for predicting the binding energies of neutral, protonated, and deprotonated water clusters. J. Chem. Theory Comput. 5, 1016–1026.
Chan, G.G., Koch, C.M., Connors, L.H., 2017. Blood proteomic profiling in inherited (ATTRm) and acquired (ATTRwt) forms of transthyretin-associated cardiac amyloidosis. J. Proteome Res. 16, 1659–1668.
Chattaraj, P.K., Roy, D.R., 2007. Update 1 of: electrophilicity index. Chem. Rev. 107, PR46–PR74.
Chen, W., Xu, T., He, F., Wang, W., Wang, C., Strzalka, J., Liu, Y., Wen, J., Miller, D.J., Chen, J., 2011. Hierarchical nanomorphologies promote exciton dissociation in polymer/fullerene bulk heterojunction solar cells. Nano Lett. 11, 3707–3713.
Conibeer, G., 2007. Third-generation photovoltaics. Mater. Today 10, 42–50.
Conibeer, G., Green, M., Cho, E.-C., König, D., Cho, Y.-H., Fangsuwannarak, T., Scardera, G., Pink, E., Huang, Y., Puzzer, T., 2008. Silicon quantum dot nanostructures for tandem photovoltaic cells. Thin Solid Films 516, 6748–6756.
Dennington, R., Keith, T.A., Millam, J.M., 2016. GaussView 6.0. 16. Semichem Inc.: Shawnee Mission, KS, USA.
Farhat, A., Khera, R.A., Iqbal, S., Iqbal, J., 2020. Tuning the optoelectronic properties of Subphthalocyanine (SubPc) derivatives for photovoltaic applications. Opt. Mater. 107, 110154.
Firdaus, Y., Le Corre, V.M., Karuthedath, S., Liu, W., Markina, A., Huang, W., Chattopadhyay, S., Nahid, M.M., Nugraha, M.I., Lin, Y., 2020. Long-range exciton diffusion in molecular non-fullerene acceptors. Nat. Commun. 11, 5220.
Frisch, M.J., Trucks, G.W., Schlegel, H.B., Scuseria, G.E., Robb, M. A., Cheeseman, J.R., Scalmani, G., Barone, V., Mennucci, B., Petersson, G.A., 2009. Gaussian 09, Revision D. 01, Gaussian, Inc., Wallingford CT. See also: URL: http://www.gaussian.com.
Goszczycki, P., Stadnicka, K., Brela, M.Z., Grolik, J., Ostrowska, K., 2017. Synthesis, crystal structures, and optical properties of the π-π interacting pyrrolo [2, 3-b] quinoxaline derivatives containing 2-thienyl substituent. J. Mol. Struct. 1146, 337–346.
Green, M.A., 2002. Third generation photovoltaics: solar cells for 2020 and beyond. Physica E 14, 65–70.
Green, M.A., 2004. Recent developments in photovoltaics. Sol. Energy 76, 3–8.
Hanwell, M.D., Curtis, D.E., Lonie, D.C., Vandermeersch, T., Zurek, E., Hutchison, G.R., 2012. Avogadro: an advanced semantic chemical editor, visualization, and analysis platform. J. Cheminf. 4, 1–17.
Heidarzadeh, H., Tavousi, A., 2019. Performance enhancement methods of an ultra-thin silicon solar cell using different shapes of back grating and angle of incidence light. Mater. Sci. Eng. B 240, 1–6.
Irfan, M., Iqbal, J., Sadaf, S., Eliasson, B., Rana, U.A., Ud-din Khan, S., Ayub, K., 2017. Design of donor–acceptor–donor (D–A–D) type small molecule donor materials with efficient photovoltaic parameters. Int. J. Quantum Chem 117, e25363.
Janjua, M.R.S.A., 2012. Quantum mechanical design of efficient second-order nonlinear optical materials based on heteroaromatic imido-substituted hexamolybdates: First theoretical framework of POM-based heterocyclic aromatic rings. Inorg. Chem. 51, 11306–11314.
Janjua, M.R.S.A., Amin, M., Ali, M., Bashir, B., Khan, M.U., Iqbal, M.A., Guan, W., Yan, L., Su, Z.-M., 2012a. A DFT study on the two-dimensional second-order nonlinear optical (NLO) response of terpyridine-substituted hexamolybdates: physical insight on 2D inorganic–organic hybrid functional materials. Eur. J. Inorg. Chem. 2012, 705–711.
Janjua, M.R.S.A., Khan, M.U., Bashir, B., Iqbal, M.A., Song, Y., Naqvi, S.A.R., Khan, Z.A., 2012b. Effect of π-conjugation spacer (CC) on the first hyperpolarizabilities of polymeric chain containing polyoxometalate cluster as a side-chain pendant: A DFT study. Comput. Theor. Chem. 994, 34–40.
Javed, I., Khurshid, A., Arshad, M.N., Wang, Y., 2014. Photophysical and electrochemical properties and temperature dependent geometrical isomerism in alkyl quinacridonediimines. New J. Chem. 38, 752–761.
Kayani, K.Q., Yaqoob, U., Jabeen, S., Iqbal, S., Yaseen, M., Khalid, M., Akhter, M.S., Iqbal, J., 2021. Tris-isopropyl-sily-ethynyl anthracene based small molecules for organic solar cells with efficient photovoltaic parameters. Comput. Theor. Chem. 1202, 113305.
Khalid, M., Ali, A., Jawaria, R., Asghar, M.A., Asim, S., Khan, M.U., Hussain, R., ur Rehman, M.F., Ennis, C.J., Akram, M.S., 2020a. First principles study of electronic and nonlinear optical properties of A-D–π–A and D–A–D–π–A configured compounds containing novel quinoline–carbazole derivatives. RSC Adv. 10, 22273–22283.
Khalid, M., Khera, R.A., Jabeen, S., Langer, P., Iqbal, J., 2020b. Designing 2D fused ring materials for small molecules organic solar cells. Comput. Theor. Chem. 1183, 112848.
Khalid, M., Ahmed, R., Shafiq, I., Arshad, M., Asghar, M.A., Munawar, K.S., Imran, M., Braga, A.A., 2022a. First theoretical framework for highly efficient photovoltaic parameters by structural modification with benzothiophene-incorporated acceptors in dithiophene based chromophores. Sci. Rep. 12, 20148.
Khalid, M., Arshad, M.N., Murtaza, S., Shafiq, I., Haroon, M., Asiri, A.M., de AlcântaraMorais, S.F., Braga, A.A., 2022b. Enriching NLO efficacy via designing non-fullerene molecules with the modification of acceptor moieties into ICIF2F: an emerging theoretical approach. RSC Adv. 12, 13412–13427.
Khalid, M., Khan, M., Mahmood, K., Arshad, M., Imran, M., Braga, A.A.C., Hussain, R., 2022c. Theoretical designing of non-fullerene derived organic heterocyclic compounds with enhanced nonlinear optical amplitude: a DFT based prediction. Sci. Rep. 12, 20220.
Khan, M.U., Khalid, M., Ibrahim, M., Braga, A.A.C., Safdar, M., Al-Saadi, A.A., Janjua, M.R.S.A., 2018. First theoretical framework of triphenylamine–dicyanovinylene-based nonlinear optical dyes: structural modification of π-linkers. J. Phys. Chem. C 122, 4009–4018.
Khan, M.U., Ibrahim, M., Khalid, M., Braga, A.A.C., Ahmed, S., Sultan, A., 2019a. Prediction of second-order nonlinear optical properties of D–π–A compounds containing novel fluorene derivatives: a promising route to giant hyperpolarizabilities. J. Clust. Sci. 30, 415–430.
Khan, M.U., Ibrahim, M., Khalid, M., Qureshi, M.S., Gulzar, T., Zia, K.M., Al-Saadi, A.A., Janjua, M.R.S.A., 2019b. First theoretical probe for efficient enhancement of nonlinear optical properties of quinacridone based compounds through various modifications. Chem. Phys. Lett. 715, 222–230.
Khan, M.U., Iqbal, J., Khalid, M., Hussain, R., Braga, A.A.C., Hussain, M., Muhammad, S., 2019c. Designing triazatruxene-based donor materials with promising photovoltaic parameters for organic solar cells. RSC Adv. 9, 26402–26418.
Khan, M.U., Hussain, R., Yasir Mehboob, M., Khalid, M., Shafiq, Z., Aslam, M., Al-Saadi, A.A., Jamil, S., Janjua, M.R.S.A., 2020. In silico modeling of new "Y-Series"-based near-infrared sensitive non-fullerene acceptors for efficient organic solar cells. ACS Omega 5, 24125–24137.
Khan, M.U., Khalid, M., Hussain, R., Umar, A., Mehboob, M.Y., Shafiq, Z., Imran, M., Irfan, A., 2021a. Novel W-shaped oxygen heterocycle-fused fluorene-based non-fullerene acceptors: first the-

oretical framework for designing environment-friendly organic solar cells. Energy Fuel 35, 12436–12450.
Khan, M.U., Mehboob, M.Y., Hussain, R., Fatima, R., Tahir, M.S., Khalid, M., Braga, A.A.C., 2021b. Molecular designing of high-performance 3D star-shaped electron acceptors containing a truxene core for nonfullerene organic solar cells. J. Phys. Org. Chem. 34, e4119.
Koopmans, T., 1934. Über die Zuordnung von Wellenfunktionen und Eigenwerten zu den einzelnen Elektronen eines Atoms. Physica 1, 104–113.
Köse, M.E., 2012. Evaluation of acceptor strength in thiophene coupled donor–acceptor chromophores for optimal design of organic photovoltaic materials. Chem. A Eur. J. 116, 12503–12509.
Köse, M.E., Mitchell, W.J., Kopidakis, N., Chang, C.H., Shaheen, S. E., Kim, K., Rumbles, G., 2007. Theoretical studies on conjugated phenyl-cored thiophene dendrimers for photovoltaic applications. J. Am. Chem. Soc. 129, 14257–14270.
Lin, Y., Adilbekova, B., Firdaus, Y., Yengel, E., Faber, H., Sajjad, M., Zheng, X., Yarali, E., Seitkhan, A., Bakr, O.M., 2019. 17% efficient organic solar cells based on liquid exfoliated WS2 as a replacement for PEDOT: PSS. Adv. Mater. 31, 1902965.
Lu, T., Chen, F., 2012. Multiwfn: A multifunctional wavefunction analyzer. J. Comput. Chem. 33, 580–592.
Mahmood, A., Hu, J.-Y., Xiao, B., Tang, A., Wang, X., Zhou, E., 2018. Recent progress in porphyrin-based materials for organic solar cells. J. Mater. Chem. A 6, 16769–16797.
Mandado, M., Blockhuys, F., Van Alsenoy, C., 2006. On the applicability of QTAIM, Hirshfeld and Mulliken delocalisation indices as a measure of proton spin–spin coupling in aromatic compounds. Chem. Phys. Lett. 430, 454–458.
Mehboob, M.Y., Adnan, M., Hussain, R., Irshad, Z., 2021a. Quantum chemical designing of banana-shaped acceptor materials with outstanding photovoltaic properties for high-performance non-fullerene organic solar cells. Synth. Met. 277, 116800.
Mehboob, M.Y., Hussain, R., Khan, M.U., Adnan, M., Ehsan, M.A., Rehman, A., Janjua, M.R.S.A., 2021b. Quantum chemical design of near-infrared sensitive fused ring electron acceptors containing selenophene as π-bridge for high-performance organic solar cells. J. Phys. Org. Chem. 34, e4204.
Mehboob, M.Y., Khan, M.U., Hussain, R., Ayub, K., Sattar, A., Ahmad, M.K., Irshad, Z., Adnan, M., 2021c. Designing of benzodithiophene core-based small molecular acceptors for efficient non-fullerene organic solar cells. Spectrochim. Acta A Mol. Biomol. Spectrosc. 244, 118873.
Mustafa, G., Shafiq, I., Shaikh, Q., Mustafa, A., Zahid, R., Rasool, F., Asghar, M.A., Baby, R., Alshehri, S.M., Haroon, M., 2023. Quantum chemical exploration of A- π1–D1–π2–D2-Type compounds for the exploration of chemical reactivity, optoelectronic, and third-order nonlinear optical properties. ACS Omega.
O'boyle, N.M., Tenderholt, A.L., Langner, K.M., 2008. Cclib: a library for package-independent computational chemistry algorithms. J. Comput. Chem. 29, 839–845.
Parr, R.G., Donnelly, R.A., Levy, M., Palke, W.E., 1978. Electronegativity: the density functional viewpoint. J. Chem. Phys. 68, 3801–3807.
Parr, R.G., Szentpály, L., Liu, S., 1999. Electrophilicity index. J. Am. Chem. Soc. 121, 1922–1924.
Pearson, R.G., 1986. Absolute electronegativity and hardness correlated with molecular orbital theory. Proc. Natl. Acad. Sci. 83, 8440–8441.
Pearson, R.G., 2005. Chemical hardness and density functional theory. J. Chem. Sci. 117, 369–377.
Peng, Z., Yu, L., 1994. Second-order nonlinear optical polyimide with high-temperature stability. Macromolecules 27, 2638–2640.
Saleem, R., Farhat, A., Khera, R.A., Langer, P., Iqbal, J., 2021. Designing of small molecule non-fullerene acceptors with cyanobenzene core for photovoltaic application. Comput. Theor. Chem. 1197, 113154.
Scharber, M.C., Mühlbacher, D., Koppe, M., Denk, P., Waldauf, C., Heeger, A.J., Brabec, C.J., 2006. Design rules for donors in bulk-heterojunction solar cells—Towards 10% energy-conversion efficiency. Adv. Mater. 18, 789–794.
Shafiq, I., Khalid, M., Asghar, M.A., Adeel, M., ur Rehman, M.F., Syed, A., Bahkali, A.H., Elgorban, A.M., Akram, M.S., 2023a. Exploration of photovoltaic behavior of benzodithiophene based non-fullerene chromophores: first theoretical framework for highly efficient photovoltaic parameters. J. Mater. Res. Technol. 24, 1882–1896.
Shafiq, I., Khalid, M., Muneer, M., Asghar, M.A., Baby, R., Ahmed, S., Ahamad, T., de Alcântara Morais, S.F., Braga, A.A., 2023b. The impact of structural modifications into benzodithiophene compounds on electronic and optical properties for organic solar cells. Mater. Chem. Phys. 308, 128154.
Sheela, N.R., Muthu, S., Sampathkrishnan, S., 2014. Molecular orbital studies (hardness, chemical potential and electrophilicity), vibrational investigation and theoretical NBO analysis of 4–4′-(1H–1, 2, 4-triazol-1-yl methylene) dibenzonitrile based on abinitio and DFT methods. Spectrochim. Acta A Mol. Biomol. Spectrosc. 120, 237–251.
Siddique, M.B.A., Hussain, R., Siddique, S.A., Mehboob, M.Y., Irshad, Z., Iqbal, J., Adnan, M., 2020. Designing triphenylamine-configured donor materials with promising photovoltaic properties for highly efficient organic solar cells. ChemistrySelect 5, 7358–7369.
Sun, C., Pan, F., Bin, H., Zhang, J., Xue, L., Qiu, B., Wei, Z., Zhang, Z.-G., Li, Y., 2018. A low cost and high performance polymer donor material for polymer solar cells. Nat. Commun. 9, 743.
Szukalski, A., Sahraoui, B., Kulyk, B., Lazar, C.A., Manea, A.M., Mysliwiec, J., 2017. Chemical structure versus second-order nonlinear optical response of the push–pull type pyrazoline-based chromophores. RSC Adv. 7, 9941–9947.
Tahir, M.N., Khalid, M., Islam, A., Mashhadi, S.M.A., Braga, A.A., 2017. Facile synthesis, single crystal analysis, and computational studies of sulfanilamide derivatives. J. Mol. Struct. 1127, 766–776.
Tang, S., Zhang, J., 2012. Design of donors with broad absorption regions and suitable frontier molecular orbitals to match typical acceptors via substitution on oligo (thienylenevinylene) toward solar cells. J. Comput. Chem. 33, 1353–1363.
Tavousi, A., 2019. Wavelength-division demultiplexer based on heterostructure octagonal-shape photonic crystal ring resonators. Optik 179, 1169–1179.
Toro-Labbé, A., 1999. Characterization of chemical reactions from the profiles of energy, chemical potential, and hardness. Chem. A Eur. J. 103, 4398–4403.
Traverse, C.J., Pandey, R., Barr, M.C., Lunt, R.R., 2017. Emergence of highly transparent photovoltaics for distributed applications. Nat. Energy 2, 849–860.
ul Ain, Q., Shehzad, R.A., Yaqoob, U., Sharif, A., Sajid, Z., Rafiq, S., Iqbal, S., Khalid, M., Iqbal, J., 2021. Designing of benzodithiophene acridine based Donor materials with favorable photovoltaic parameters for efficient organic solar cell. Comput. Theor. Chem. 1200, 113238.
UrRehman, S., Anwer, M., BiBi, S., Jamil, S., Yasin, M., Khan, S.R., Nadeem, R., Ali, S., Jia, R., 2022. DFT analysis of different substitutions on optoelectronic properties of carbazole-based small acceptor materials for Organic Photovoltaics. Mater. Sci. Semicond. Process. 140, 106381.
Wu, L., Tian, W., Jiang, X., 2005. Silicon-based solar cell system with a hybrid PV module. Sol. Energy Mater. Sol. Cells 87, 637–645.

Xu, X., Feng, K., Bi, Z., Ma, W., Zhang, G., Peng, Q., 2019. Single-junction polymer solar cells with 16.35% efficiency enabled by a platinum (II) complexation strategy. Adv. Mater. 31, 1901872.

Yan, J., Saunders, B.R., 2014. Third-generation solar cells: a review and comparison of polymer: fullerene, hybrid polymer and perovskite solar cells. RSC Adv. 4, 43286–43314.

Yaqoob, U., Ayub, A.R., Rafiq, S., Khalid, M., El-Badry, Y.A., El-Bahy, Z.M., Iqbal, J., 2021. Structural, optical and photovoltaic properties of unfused Non-Fullerene acceptors for efficient solution processable organic solar cell (Estimated PCE greater than 12.4%): A DFT approach. J. Mol. Liq. 341, 117428.

Yu, G., Gao, J., Hummelen, J.C., Wudl, F., Heeger, A.J., 1995. Polymer photovoltaic cells: enhanced efficiencies via a network of internal donor-acceptor heterojunctions. Science 270, 1789–1791.

Zhan, X., Marder, S.R., 2019. Non-fullerene acceptors inaugurating a new era of organic photovoltaic research and technology. Mater. Chem. Front. 3, 180.

Zhang, Y., Liu, Z., Shan, T., Wang, Y., Zhu, L., Li, T., Liu, F., Zhong, H., 2020. Tuning molecular geometry and packing mode of non-fullerene acceptors by alternating bridge atoms towards efficient organic solar cells. Mater. Chem. Front. 4, 2462–2471.

Zheng, Z., Yao, H., Ye, L., Xu, Y., Zhang, S., Hou, J., 2020. PBDB-T and its derivatives: A family of polymer donors enables over 17% efficiency in organic photovoltaics. Mater. Today 35, 115–130.

Zhurko, G.A., Zhurko, D.A., 2009. ChemCraft, version 1.6. URL: http://www.chemcraftprog.com.